ACS Catalysis

Research Article

Cite This: ACS Catal. 2018, 8, 4583−4590

pubs.acs.org/acscatalysis

Boosting Photocatalytic Hydrogen Production of Porphyrinic MOFs: The Metal Location in Metalloporphyrin Matters

Fucheng Leng,[†,§] Hang Liu,[†,§] Meili Ding,[†] Qi-Pu Lin,[‡] and Hai-Long Jiang*[,†]

[†]Hefei National Laboratory for Physical Sciences at the Microscale, CAS Key Laboratory of Soft Matter Chemistry, Collaborative Innovation Center of Suzhou Nano Science and Technology, School of Chemistry and Materials Science, University of Science and Technology of China, Hefei, Anhui 230026, People's Republic of China

[‡]State Key Laboratory of Structural Chemistry, Fujian Institute of Research on the Structure of Matter, Chinese Academy of Sciences, Fuzhou, Fujian 350002, People's Republic of China

Supporting Information

ABSTRACT: Metal−organic frameworks (MOFs) have demonstrated great potentials toward catalysis, particularly in the establishment of structure−property relationships. Herein, an unusual OOP (out-of-plane) porphyrin-based MOF, synthesized by controlling the metal ion release with an unprecedented $In(OH)_3$ precursor, possesses high stability and exhibits unexpectedly high photocatalytic hydrogen production activity, far surpassing the isostructural in-plane porphyrin-based MOF counterparts. In the MOF structure, indium ions not only form indium−oxo chains but also metalate the porphyrin rings in situ, locating above the porphyrin plane instead of fitting in a coplanar fashion into the cavity and affording an unusual OOP porphyrin. Control experiments demonstrate that the OOP In(III) ions readily detach from the porphyrin rings under light excitation, avoiding the fast back electron transfer and thus greatly improving electron−hole separation efficiency and photocatalytic performance. To our knowledge, this is an unprecedented report on boosting MOF photocatalysis on the basis of special metalloporphyrin behavior.

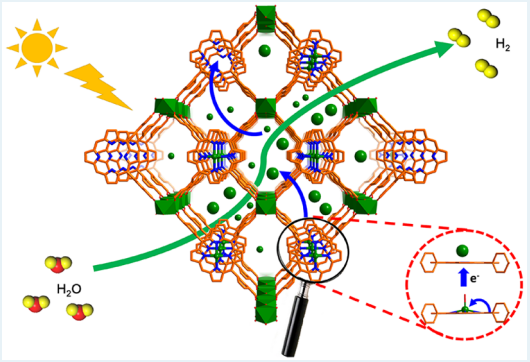

KEYWORDS: *metal−organic framework, porphyrin, metalloporphyrin, out of plane, photocatalysis, hydrogen production*

1. INTRODUCTION

The depletion of fossil energy resources and increasing environmental issues greatly motivate the development of renewable clean energy. It is very promising to convert solar energy into hydrogen fuel, especially photocatalytic hydrogen (H_2) production from water splitting.[1−6] Up to now, a variety of materials have been exploited for this process.[1−6] Among them, metal−organic frameworks (MOFs),[7−11] a relatively new class of porous materials, possess great potential in photocatalysis on account of their semiconductor-like behaviors and accessible active sites as well as the inhibited charge recombination, thanks to their porous and crystalline nature.[12−32] The tailorable, diversified, and well-defined structures of MOFs allow an in-depth understanding of structure−photocatalytic property relationships and further rational optimization of catalytic performance.

Given that UV light accounts for ∼4% while visible light contributes ∼43% of solar energy, it would be of great importance to employ MOFs that are able to harvest visible light as much as possible.[12,29] To this end, the porphyrin unit, which has been demonstrated to possess excellent performance toward hydrogen evolution,[33−37] was introduced to MOF structures due to its excellent visible light harvesting capability and some important considerations (see discussions in the Supporting Information), thus exhibiting impressive activities toward visible light photocatalytic CO_2 reduction and organic transformation.[24,25,38,39] Surprisingly, there have been only two reports on photocatalytic water splitting over porphyrinic MOFs,[14,28] possibly due to their poor stability in most cases. To fabricate chemically stable MOFs for photocatalysis, the formation of strong coordination bonds between metal ions with high charge/radius ratio (such as Zr^{4+}, Al^{3+}, In^{3+}, Fe^{3+}, etc.) and porphyrinic carboxylates based on hard−soft acid−base (HSAB) theory has been established. Among these potential metals, In^{3+} and Fe^{3+} are very promising, as not only would they afford stable skeletons but also, more importantly, they might be implanted in situ into the porphyrin centers to improve the catalytic activity.[38,40,41]

Bearing the above considerations in mind, we have successfully prepared an indium-based porphyrinic MOF, **USTC-8(In)**, in which 1D In−oxo chains are formed and connected by the porphyrin ligand to give the 3D structure. Meanwhile, additional In^{3+} ions in the structure are located above the porphyrin plane (that is, out of plane, denoted as OOP) instead of fitting in a coplanar fashion into the cavity (that is, in-plane) because of their large size (Figure S1).

Received: February 24, 2018
Revised: April 10, 2018
Published: April 13, 2018

DOI: 10.1021/acscatal.8b00764
ACS Catal. 2018, 8, 4583−4590

Thanks to the formation of strong coordination bonds, the MOF possesses very high stability in aqueous solution with pH ranging from 2 to 11. Remarkably, **USTC-8(In)** exhibits excellent photocatalytic H_2 production activity under visible light irradiation, far superior to the isostructural porphyrinic MOF counterparts with in-plane central metals. Control experiments indicate a detachment−insertion mechanism involved in the catalytic process, where the OOP In^{3+} ions detach from the porphyrin ligands under excitation, avoiding the fast back electron transfer in common metalloporphyrinic MOFs and thus greatly improving electron−hole (simply denoted e-h) separation and photocatalytic efficiency. To our knowledge, this is the first report on the unique light-induced metalloporphyrin behavior for improved e-h separation in MOF photocatalysis.

2. EXPERIMENTAL SECTION

2.1. Materials and Instrumentation. All of the chemicals were purchased from commercial sources without further treatment. The tetrakis(4-carboxyphenyl)porphyrin (TCPP) and metal-involved TCPP (M-TCPP) ligands were prepared according to previous reports.[25,42] Deionized water with a specific resistance of 18.25 MΩ·cm was obtained by reverse osmosis followed by ion exchange and filtration (Cleaned Water Treatment Co., Ltd., Hefei). Powder X-ray diffraction (XRD) patterns were measured on a Japan Rigaku Miniflex 600 rotating anode X-ray diffractometer or Holland X'Pert PRO fixed anode X-ray diffractometer equipped with graphite-monochromated Cu Kα radiation (λ = 1.54178 Å). The transmission electron microscopy (TEM) images were acquired on a JEOL JEM-2100F field-emission transmission electron microscope. Nitrogen adsorption−desorption isotherms were measured using a Micromeritics ASAP 2020 system at 77 K. Both UV−vis absorption and diffuse reflectance spectra were recorded on an UV−vis spectrophotometer (UV-2700, Shimadzu) in the wavelength range of 200−800 nm. The catalytic reaction products were analyzed and identified by gas chromatography (Shimadzu GC-2014). ^{1}H NMR spectra were recorded on a Bruker AC-400FT spectrometer (400 MHz). Thermogravimetric (TG) analysis was carried out on a TGA Q5000 integration thermal analyzer from room temperature to 700 °C at a rate of 5 °C min^{-1} under N_2 flow.

2.2. Synthesis of USTC-8. *2.2.1. Synthesis of **USTC-8(In)**.* Typically, DMF (2 mL) and HNO_3 (0.35 mL) were placed in a 5 mL glass vial with indium(III) hydroxide (6.5 mg, 0.039 mmol) and H_2TCPP (10 mg, 0.013 mmol), and the glass vial was sonicated until the ligand was completely dissolved. Then the vial was placed in a preheated oven at 120 °C for 4 days. After the mixture was cooled to room temperature, purple spindle single crystals were obtained (4.7 mg, 32%). FTIR (cm^{-1}, KBr): 3427 (w), 2923 (w), 2493 (w), 1588 (s), 1538 (m), 1399 (vs), 1177 (w), 1011 (m), 867 (w), 839 (w), 778 (m), 723 (m). Anal. Calcd for **USTC-8(In)**: C, 49.65; H, 2.08; N, 4.8. Found: C, 48.93; H, 2.36; N, 4.84.

*2.2.2. Synthesis of **USTC-8(Cu)**.* Typically, DMF (2 mL) and HNO_3 (0.3 mL) were placed in a 5 mL glass vial with indium(III) hydroxide (5 mg, 0.032 mmol) and Cu-TCPP (10 mg, 0.012 mmol) and the glass vial was sonicated until the ligand was completely dissolved. Then the vial was placed in a preheated oven at 130 °C for 2 days. After the mixture was cooled to room temperature, black spindle single crystals were obtained (5.2 mg, 37% yield). FTIR (cm^{-1}, KBr): 3413 (w), 2925 (w), 1610 (m), 1543 (m), 1402 (vs), 1179 (w), 1011 (vs), 870 (m), 839 (w), 777 (m), 722 (m). Anal. Calcd for **USTC-8(Cu)**: C, 51.94; H, 2.18; N, 5.05. Found: C, 49.65; H, 2.49; N, 4.64.

*2.2.3. Synthesis of **USTC-8(Ni)**.* Typically, DMF (2 mL) and HNO_3 (0.2 mL) were placed in a 5 mL glass vial with indium(III) hydroxide (5 mg, 0.032 mmol) and Ni-TCPP (10 mg, 0.012 mmol) and the glass vial was sonicated until the ligand was completely dissolved. Then the vial was placed in a preheated oven at 140 °C for 1 day. After the mixture was cooled to room temperature, violet spindle single crystals were obtained (4.6 mg, 33%). FTIR (cm^{-1}, KBr): 3431 (m), 2928 (w), 2350 (w), 1595 (s), 1535 (m), 1409 (vs), 1181 (w), 1007 (m), 871 (w), 829 (w), 778 (m), 716 (m). Anal. Calcd for **USTC-8(Ni)**: C, 52.17; H, 2.19; N, 5.1. Found: C, 52.09; H, 2.85; N, 4.05.

*2.2.4. Synthesis of **USTC-8(Co)** Single Crystals.* Typically, DMF (2 mL) and HNO_3 (0.3 mL) were placed in a 5 mL glass vial with indium(III) hydroxide (8 mg, 0.052 mmol) and Co-TCPP (10 mg, 0.012 mmol) and the glass vial was sonicated until the ligand was completely dissolved. Then the vial was placed in a preheated oven at 100 °C for 2 days. After the mixture was cooled to room temperature, black spindle single crystals were obtained.

*2.2.5. Synthesis of **USTC-8(Co)** Powder.* Typically, DMF (2 mL) and HNO_3 (0.3 mL) were placed in a 5 mL glass vial with indium(III) nitrate (10 mg, 0.033 mmol) and Co-TCPP (10 mg, 0.012 mmol) and the glass vial was sonicated until the ligand was dissolved completely. Then the vial was placed in a preheated oven at 100 °C for 2 days. After the mixture was cooled to room temperature, the black powder was obtained. FTIR (cm^{-1}, KBr): 3448 (m), 2913 (w), 2362 (w), 1596 (s), 1534 (m), 1391 (vs), 1176 (w), 1001 (m), 871 (w), 828 (w), 779 (m), 717 (m). Anal. Calcd for **USTC-8(Co)**: C, 51.41; H, 2.16; N, 5.00. Found: C, 51.97; H, 3.85; N, 4.49.

*2.2.6. Synthesis of **USTC-8(0.2In)**.* Typically, DMF (2 mL) and HNO_3 (0.35 mL) were placed in a 5 mL glass vial with indium(III) nitrate (2.5 mg, 0.008 mmol) and H_2TCPP (5 mg, 0.007 mmol) and the glass vial was sonicated until the solid was completely dissolved. Then the vial was placed in a preheated oven at 100 °C for 1 day. After the mixture was cooled to room temperature, purple spindle single crystals were obtained (1.2 mg, 17%). FTIR (cm^{-1}, KBr): 3319 (w), 2917 (w), 1587 (s), 1537 (m), 1408 (vs), 1179 (w), 1010 (m), 870 (w), 837 (w), 797 (m), 767 (m), 720 (m). Anal. Calcd for **USTC-8(0.2In)**: C, 54.87; H, 2.29; N, 5.33. Found: C, 54.57; H, 2.66; N, 4.88.

*2.2.7. Synthesis of **USTC-8(Cd)**.* Typically, 30 mg of **USTC-8(0.2In)** and 150 mg of $CdCl_2$ were added to 8 mL of DMF and heated in 120 °C for 12 h. After that, the liquid was decanted carefully. After three washes with DMF and two washes with acetone, the solid was dried in a vacuum drying oven. FTIR (cm^{-1}, KBr): 3439 (w), 3019 (w), 1697 (w), 1642 (s), 1600 (w), 1534 (w), 1527 (w), 1504 (w), 1405 (vs), 1179 (w), 1103 (w), 1009 (m), 980 (w), 868 (w), 833 (w), 797 (m), 772 (m), 714 (m). Anal. Calcd for **USTC-8(Cd)**: C, 49.73; H, 2.09; N, 4.83. Found: C, 48.93; H, 2.36; N, 4.84. ICP-AES results for **USTC-8(Cd)**: In, 21.3 wt %; Cd, 8.7 wt % (calculated: In, 22.20 wt %; Cd, 7.9 wt %).

2.3. Crystallographic Data. The single-crystal X-ray diffraction data for the **USTC-8** series were collected using the synchrotron radiation X-ray source at 173 K, λ = 0.65250 Å, at the Shanghai Synchrotron Radiation Facility. The crystal structures were solved by direct methods and refined by full matrix least-squares methods against F^2 using the SHELXL-97

DOI: 10.1021/acscatal.8b00764
ACS Catal. 2018, 8, 4583−4590

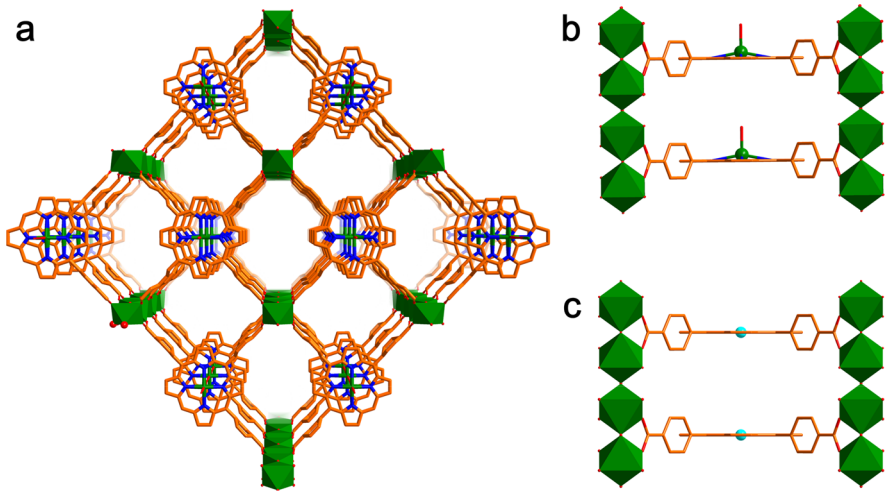

Figure 1. (a) View of the 3D network of **USTC-8(In)** along the *a* axis. Views of partial structures in (b) **USTC-8(In)** and (c) **USTC-8(M)** (M = Cu, Co, Ni), highlighting the metal location at metalloporphyrin motif involved in the MOF structure. The framework is represented by a wire model, and the metal atoms at metalloporphyrins are represented by a ball-and-stick model. The $InO_4(OH)_2$ polyhedra are shaded in olive green. The In, Cu, C, O, and N are shown as green, cyan, orange, red, and blue circles, respectively. Hydrogen atoms are omitted for clarity.

program package and Olex-2 software.[43−45] All of the non-hydrogen atoms were refined with anisotropic displacement parameters, and the positions of hydrogens were fixed at calculated positions and refined isotropically. The solvent molecules in **USTC-8(Cu)**, **USTC-8(Co)**, and **USTC-8(Ni)** are highly disordered and hard to be refined by using conventional discrete-atom models. Hence, the contribution of solvent electron densities was removed by the SQUEEZE routine in PLATON.[46] The crystallographic data and structure refinement for the **USTC-8** series are summarized in Tables S1 and S2. These data can be obtained free of charge from The Cambridge Crystallographic Data Centre.

2.4. Characterization for the Occupancy of In2 in USTC-8(0.2In) and USTC-8(In). The samples were treated by using a previously reported method.[38] Typically, ∼2 mg of activated sample was placed in DMSO-d_6 (500 μL) and digested with 50 μL of diluted DCl (35 wt % DCl in D_2O). The samples were sonicated to ensure complete dissolution to give the corresponding ^{1}H NMR spectra.

2.5. Sample Activation and N_2 Adsorption Measurements. The as-synthesized **USTC-8** (∼50 mg) sample was washed three times with DMF and two times with acetone. After that, it was soaked in acetone for 12 h. After the centrifugation and decantation of the supernatant, the samples were separated by centrifugation and then activated under vacuum for 12 h. Before the adsorption measurements, the sample was dried through the "degas" function of the adsorption instrument for 12 h at 140 °C.

2.6. Chemical Stability Test for USTC-8(In). pH 1, 2, 3, 10, 11, and 12 aqueous solutions were prepared, and 5 mg of the sample was soaked in each solution for 12 h. After that, all of the samples were centrifuged, washed three times with acetone, and dried in the oven for further PXRD measurement.

2.7. UV−Vis Absorption Spectra Changes of MOF Suspension Solution under Light. A trace sample was added to a prepared solution (CH_3CN/H_2O/TEA = 1/1/0.1) and dispersed thoroughly. Then the solution was divided into two parts, one was placed in darkness while the other was irradiated by the Xe lamp for a few minutes. After that, UV−vis absorption spectra for these two solutions were tested immediately.

2.8. Photocatalytic Activity Evaluation. Typically, 10 mg of activated **USTC-8** sample was dispersed in a mixed solution of 23 mL of acetonitrile, 0.5 mL of deionized water, and 2 mL of trimethylamine (TEA). After that, the suspension solution was placed in a 160 mL optical reaction vessel (purchased from Perfect Light) with flowing tap water. Then, the suspension was stirred and purged for 40 min to remove the air. After H_2PtCl_6 was introduced (Pt content: 1.5 wt %), the photocatalysis reaction was carried out using a 300 W Xe lamp (LX-300F) equipped with a UV cutoff filter (λ >380 nm) with stirring. Hydrogen gas was measured by gas chromatography (Shimadzu GC-2014, nitrogen as a carrier gas) using a thermal conductivity detector (TCD). For each evaluation of hydrogen generation, 200 μL of the headspace was injected into the GC and was quantified by a calibration plot to the internal hydrogen standard.

2.9. Mott−Schottky Plot Measurements. Typically, an activated **USTC-8** sample (2 mg) was added to a solution of 10 μL of 5 wt % Nafion and 1.5 mL of ethanol and then dispersed thoroughly. After that 20 μL of the suspension solution was dropped on a glassy-carbon electrode to prepare the working electrode. Mott−Schottky plots were measured on an electrochemical workstation (Zahner Zennium) in a standard three-electrode system with Ag/AgCl as the reference electrode at frequencies of 500, 1000, and 1500 Hz, respectively. A 0.1 M deoxygenated Na_2SO_4 solution was used as the electrolyte.

2.10. Photocurrent Measurements. Typically, an activated **USTC-8** sample (2 mg) was added to a solution of 10 μL of 5 wt % Nafion and 1.5 mL of ethanol and then dispersed thoroughly. After that 50 μL of the suspension solution was dropped on ITO and dried at room temperature to prepare the working electrode. Photocurrent measurements were performed on a CHI 760E electrochemical workstation (Chenhua Instrument, Shanghai, People's Republic of China) in a standard three-electrode system with MOF-coated ITO as the working electrode, Pt plate as the counter electrode, and Ag/AgCl as a reference electrode. A 300 W Xe lamp with a UV cutoff filter (λ >380 nm) was used as the light source. Photoresponsive signals of the samples were measured under chopped light with a bias potential of +0.6 V. A 0.1 M Na_2SO_4 aqueous solution was used as the electrolyte.

DOI: 10.1021/acscatal.8b00764
ACS Catal. 2018, 8, 4583−4590

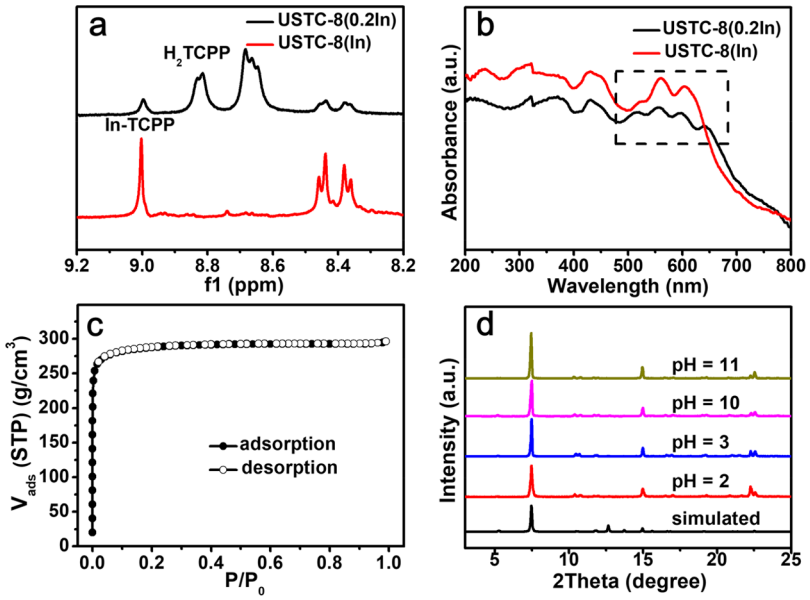

Figure 2. (a) ^{1}H NMR spectra of digested crystals of **USTC-8(0.2In)** and **USTC-8(In)**. (b) UV−vis spectra of **USTC-8(0.2In)** and **USTC-8(In)**. Their Q bands are highlighted by a dashed rectangle. (c) N_2 sorption isotherms of **USTC-8(In)** at 77 K. (d) Powder XRD profiles of **USTC-8(In)** after samples are soaked in acidic or basic solutions for 12 h.

2.11. Electrochemical Impedance Spectroscopy Measurements. The electrochemical impedance spectra were obtained on a Zahner Zennium electrochemical workstation in a standard three-electrode system with MOF-coated ITO as the working electrode, Pt plate as the counter electrode, and Ag/AgCl as a reference electrode. A 300 W Xenon lamp with a UV cutoff filter (>380 nm) was used as the light source. A 0.1 M Na_2SO_4 aqueous solution was used as the electrolyte. EIS measurements were performed with a bias potential of −0.4 V in the dark or with light.

3. RESULTS AND DISCUSSION

Numerous attempts at reactions between common indium(III) nitrate and H_2TCPP in DMF under solvothermal conditions usually gave powdery samples, possibly due to the very freely soluble $In(NO_3)_3$ and high reaction rate between In(III) ions and carboxylates. Lowering the concentration of indium ions has been demonstrated to be a possible way to reduce the reaction rate and give single crystals (denoted as **USTC-8(0.2In)**, Figure S2), which unfortunately have low In(III) occupancy in the porphyrin center and are obtained in a very low yield. Moreover, the reproducibility of **USTC-8(0.2In)** is not guaranteed due to the strong hygroscopicity of indium(III) nitrate. To overcome these difficulties, indium nitrate is replaced by $In(OH)_3$, which has extremely low solubility in DMF. The low concentration of In^{3+} ion during the solvothermal reaction is assumed to be the crucial factor in lowering the reaction rate and successfully affording the isostructural single crystals, namely **USTC-8(In)**, with complete occupation of the porphyrin center by In(III). During the crystal growth, $In(OH)_3$ dissolves gradually and slowly to retain the solubility equilibrium and low In^{3+} concentration (Figure S3), ensuring the high quality and improved yield of resultant single crystals. As far as we know, this is for the first time $In(OH)_3$ has been employed as a precursor to fabricate an In-based MOF thus far. Subsequently, replacing H_2TCPP with M-TCPP (M = Cu, Co, Ni) also successfully results in the corresponding **USTC-8(M)** (M = Cu, Co, Ni). Their phase purity has been verified by powder X-ray diffraction (XRD) patterns (Figures S4 and S5).

Single-crystal X-ray diffraction analyses indicate that the **USTC-8** series are isostructural (Figure 1a and Tables S1 and S2). All of them crystallize in the orthorhombic crystal system with the space group *Cmmm*. For **USTC-8(0.2In)** and **USTC-8(In)**, there are two crystallographically unique In(III) ions in the structure (Figure S6), of which In1 is pseudo-octahedrally coordinated by four oxygen atoms from four ligands in the basal plane and two oxygen atoms from μ_2-OH groups in the axial direction, leading to $InO_4(OH)_2$ chains (Figure S7), and In2 is coordinated by four nitrogen atoms coming from one porphyrin ring and a hydroxide at the axial position (Figure 1b and Figure S6). Unlike the case for common metalloporphyrins, induced by both large In(III) size and axial hydroxyl coordination,[47] In2 is located out of the plane of the porphyrin and remains ∼0.4 Å away from the porphyrin plane.[48,49] In contrast, **USTC-8(M)** (M = Cu, Co, Ni) possesses a structure almost identical with that of **USTC-8(In)** except the metal ions stay in the plane of the porphyrins (Figure 1c and Figure S8). Each carboxylate in the TCPP ligand bridges to two In1 atoms from the $InO_4(OH)_2$ chain to construct the 3D network featuring 1D channels with a size of 13.6 × 7.2 Å^2 running through the *a* axis (Figure 1a and Figure S9). The effective free volume is 53.3%, estimated by PLATON after excluding the free solvents.[46]

A closer structural analysis indicates that the occupancy of In2 in **USTC-8(In)** is possibly 100% with a U_{eq} value as low as 0.015. In contrast, the In2 occupancy in **USTC-8(0.2In)** is very low (18%) on the basis of single-crystal data. To figure out the In2 occupancy, the ligands in these MOFs were identified by ^{1}H NMR after MOF dissolution (Figure 2a).[38,50] The ^{1}H NMR spectrum of **USTC-8(In)** clearly gives a peak at 9.0 ppm attributed to hydrogen atoms from In-TCPP, whereas no peak at 8.8 ppm from free base porphyrin can be observed, demonstrating the 100% occupancy of In2 at the porphyrin center, which is extremely rare in porphyrinic In-MOFs.[38,40] However, the strong peaks at ∼8.8 ppm and the weak peak at

DOI: 10.1021/acscatal.8b00764
ACS Catal. 2018, 8, 4583−4590

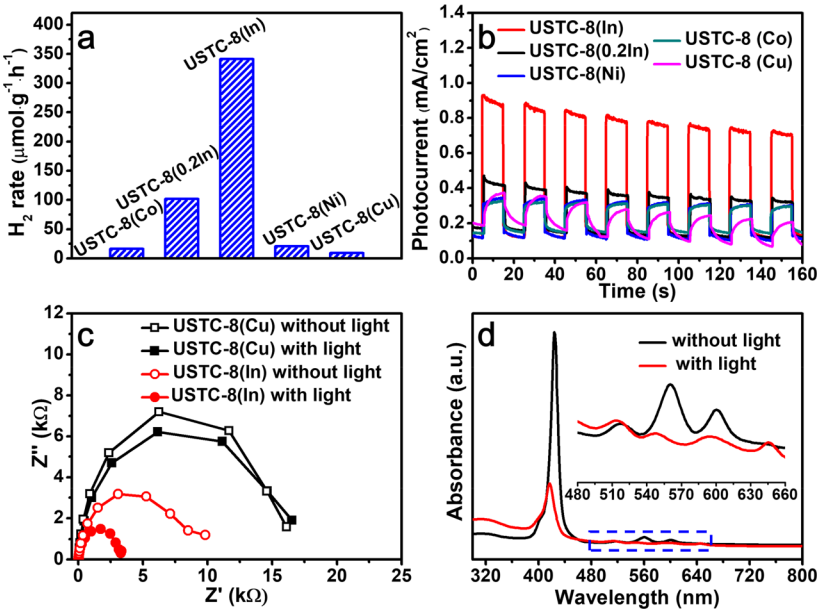

Figure 3. (a) Photocatalytic H_2 production via water splitting over different MOFs. (b) Photocurrent responses of **USTC-8** series. (c) EIS Nyquist plots of **USTC-8(M)** (M = Cu, In) in the absence or presence of light irradiation. The line is a guide for the eye and is not a fitting curve. (d) UV−vis absorption spectra of **USTC-8(In)** suspension solution with and without light irradiation. Inset: enlarged spectra of the area highlighted by a blue dashed rectangle.

~9.0 ppm in the ^{1}H NMR spectrum of **USTC-8(0.2In)** suggest the low occupancy of In2 (20%) (Figure 2a), in agreement with the results from crystallographic data. The results are further supported by UV−vis spectra, in which **USTC-8(In)** shows three peaks in the Q band assignable to OOP porphyrin (In-TCPP), while **USTC-8(0.2In)** gives four peaks reflecting free base porphyrin in the Q band (Figure 2b).[51] This significant occupancy difference of In(III) in metalloporphyrins between two MOFs indicates the merit of $In(OH)_3$ relative to the common $In(NO_3)_3$ as a precursor. To further illustrate this, the preparation of **USTC-8** with higher metalation percentage at porphyrin centers by In(III) has been attempted by introducing more $In(NO_3)_3$ precursor.[38] Accordingly, the metalation percentage can be increased to only a slight degree. Even when the concentration of $In(NO_3)_3$ is increased to as high as 10 mg/mL, the percentage of porphyrin metalation does not reach 100% and meanwhile a new phase appears, demonstrating that 100% occupancy of In2 cannot be achieved in **USTC-8** by this traditional way with $In(NO_3)_3$ as a precursor (Figures S10−S12).

N_2 sorption isotherms of **USTC-8(In)** exhibit type I microporous isotherms with a Brunauer−Emmett−Teller (BET) surface area of 1139 m^2/g (Figure 2c). The **USTC-8** series metalated with other metals in their porphyrin centers feature similar pore characters and surface areas (Figures S13−S17). All compounds in the **USTC-8** series exhibit considerable thermal stability up to 340 °C according to the thermogravimetric data (Figure S18). A chemical stability investigation for **USTC-8(In)** indicates that it remains stable in aqueous solutions over a broad pH range from 2 to 11, as evidenced by powder XRD patterns (Figure 2d). The result highlights the fact that **USTC-8(In)** is the most stable In-MOF thus far that possesses permanent pores,[40,52−54] making **USTC-8(In)** a great platform for future applications.

To elucidate the semiconductor-like behavior of the above MOFs and their possible use for photocatalytic H_2 production, Mott−Schottky measurements have been conducted at frequencies of 500, 1000, and 1500 Hz (Figures S19−S23). All positive slopes of the obtained C^{-2} values (vs the applied potentials) are indicative of n-type semiconductors. It is accepted that the flat band is equal to the conduction band (LUMO) for n-type semiconductors,[25] which is independent of the frequency and determined from the intersection of ~−0.3 V vs Ag/AgCl (i.e., −0.10 V vs NHE) for all of these MOFs. With similar band gap energies (E_g) being estimated by Tauc plots (Figures S24−S28; for example, 1.79 V for **USTC-8(In)**), their valence bands (HOMO) are accordingly obtained (Figures S19−S23, inset). Given the more negative LUMO potentials in these MOFs in comparison to the proton reduction (0 V vs NHE), it is theoretically feasible for photocatalytic H_2 production to occur. The broad UV−vis spectra for all of these MOFs also suggest their great harvesting ability for both UV and visible light (Figure 2b and Figures S29−S31).

The above results encouraged us to investigate the visible light photocatalytic activities of these MOFs. Although they share the same LUMO potential, **USTC-8** species with different metal ions at porphyrin centers exhibit distinctly different activities toward photocatalytic H_2 production (Figure 3a). Strikingly, **USTC-8(In)** displays the best photocatalytic activity (341.3 μmol g^{-1} h^{-1}) by introduction of H_2PtCl_6 to give Pt nanoparticles as a cocatalyst under visible-light irradiation (Figure S32 and Table S3), which is around 18−37 times higher than the activities of other **USTC-8(M)** (M = Co, Cu, Ni) as well as ~3.4 times **USTC-8(0.2In)** activity (Figure 3a). Thanks to their high stability, all of these MOFs present well retained framework integrity and crystallinity during the photocatalytic process (Figures S33−S37).

To elucidate the mechanism behind the exceptional activity of **USTC-8(In)**, photocurrent and electrochemical impedance spectroscopy (EIS) measurements have been carried out to unveil their e-h separation efficiency and electronic conductivity, respectively. As expected, **USTC-8(In)** shows the highest photocurrent response among all investigated MOFs

DOI: 10.1021/acscatal.8b00764
ACS Catal. 2018, 8, 4583−4590

(Figure 3b), revealing that the OOP porphyrin endows the MOF with superior charge separation efficiency. The EIS curves are found to be almost identical in the absence or presence of light irradiation for **USTC-8(M)** (M = Co, Cu, Ni) (Figure 3c and Figures S38 and S39), which indicates that their high charge-transfer resistances are not affected by light. In sharp contrast, **USTC-8(In)** manifests a much smaller radius upon light irradiation, implying its greatly reduced charge-transfer resistance under light irradiation. These results imply different processes of electron transport between OOP and in-plane porphyrin-based MOFs.

A tentative mechanism has been proposed to elucidate the superior activity of **USTC-8(In)** according to the above facts and previous reports (Figure 4).[51,55] Generally, photogenerated

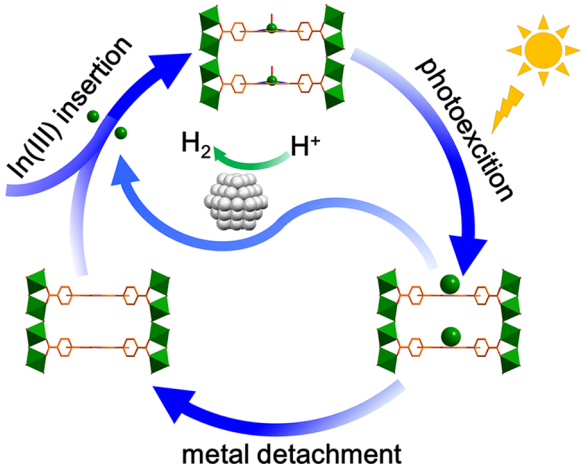

Figure 4. Proposed detachment−insertion mechanism of **USTC-8(In)** during the photocatalytic recycle.

electrons will transfer to the central metals of metalloporphyrin in MOFs upon light irradiation.[51] Then the back electron transfer would quickly occur from the metal to the ligand in common porphyrinic MOFs, such as **USTC-8(M)** (M = Co, Cu, Ni). In comparison, when electrons transfer to the OOP metals, for example, in **USTC-8(In)**, the OOP metal ions will be reduced, resulting in increased atomic size and weakened binding with the surrounding nitrogen atoms. Accordingly, the reduced indium ions carrying the electrons tend to detach from the porphyrin rings, thus avoiding the back electron transfer and e-h recombination. Serving as electron mediators, the reduced indium ions would then transfer electrons to the colloidal Pt cocatalyst. Subsequently, protons will be reduced to H_2 on platinum and the reduced indium ions will be oxidized back to In^{3+}. Meanwhile, the holes on porphyrin motifs are reduced by the sacrificial agent TEA to give the free base porphyrin, which can be converted to the original OOP porphyrin by the insertion of dissociative indium ions. It is worth noting that the recognition of **USTC-8(In)** as a photocatalyst might not be rigorous, as its structure changes with partial In(III) ions leaching out during the photocatalysis and In(III) should be reintroduced to regenerate. This is not an individual case, and the leaching of active sites constantly occurs, which changes the structure/composition of the original catalyst materials.[56−58] In fact, **USTC-8(In)** together with its leached In(III) ions as a whole, which includes both heterogeneous and homogeneous parts, should be called the photocatalyst, whose stability has been further investigated and demonstrated by five consecutive recycling experiments (Figure S40).

The proposed mechanism has been further verified by a series of experiments. Upon exposure to light for a time, the UV−vis absorption spectrum of **USTC-8(In)** suspension solution displays significant changes, e.g. the B band red shift and the increase in peaks from three to four in the Q band, indicating the In^{3+} detachment (Figure 3d and Figure S41).[51,55] In comparison, no obvious change in the Q or B band of **USTC-8(M)** (M = Cu, Ni) can be observed after light irradiation treatment (Figures S42 and S43). Apart from that, the indium ion is detectable in the supernatant solution (concentration: 4.23 $\mu g\ mL^{-1}$) after photocatalysis, again demonstrating the detachment of OOP indium ions. In addition, **USTC-8(0.2In)** presents only 29% activity of **USTC-8(In)** (Figure 3a), declaring that the high activity of **USCT-8(In)** originates from the OOP porphyrin rather than the H_2TCPP generated upon indium detachment. This argument is also supported by recycling experiments. The H_2 production rate of **USTC-8(In)** decreases significantly in the second round because of the metal detachment from the porphyrin centers. Upon regeneration of deactivated MOF by In(III) insertion, its activity can be almost recovered in the third run of catalysis (Figure S45). To further manifest the high activity of OOP porphyrin, **USTC-8(Cd)**, which might involve an OOP porphyrin according to a previous report,[59] presents much higher activity than its parent **USTC-8(0.2In)** (215.9 vs 102 $\mu mol\ g^{-1}\ h^{-1}$) (Figure S46). This result again supports that the metal position at the porphyrins accounts for the high activity of **USTC-8(In)**.

4. CONCLUSION

In summary, a highly stable OOP porphyrin-based MOF, **USTC-8(In)**, has been fabricated on the basis of controlled metal ion release with an $In(OH)_3$ precursor for the first time. The In(III) ions at the OOP porphyrin are reduced and readily detach from the porphyrin rings under light irradiation, avoiding the back electron transfer and thus inhibiting the e-h recombination. As a result, thanks to the high stability and particular OOP porphyrin structure, **USTC-8(In)** exhibits excellent photocatalytic H_2 production activity, far superior to that of the isostructural **USTC-8** with in-plane central metals as well as that of **USTC-8(0.2In)** with 20% occupancy of In(III) at porphyrin center. This work not only highlights how the metal location in metalloporphyrins in MOFs affects the photocatalytic efficiency but also offers a novel perspective to understand the role of metalloporphyrins in photocatalysis.

■ ASSOCIATED CONTENT

Supporting Information

The Supporting Information is available free of charge on the ACS Publications website at DOI: 10.1021/acscatal.8b00764.

Full experimental details and characterization data (PDF)
Crystallographic data (CIF)
Crystallographic data (CIF)
Crystallographic data (CIF)
Crystallographic data (CIF)
Crystallographic data (CIF)

■ AUTHOR INFORMATION

Corresponding Author

*E-mail for H.L.-J.: jianglab@ustc.edu.cn.

DOI: 10.1021/acscatal.8b00764
ACS Catal. 2018, 8, 4583−4590

ORCID

Qi-Pu Lin: 0000-0002-7723-3676
Hai-Long Jiang: 0000-0002-2975-7977

Author Contributions

[§]F.L. and H.L. contributed equally to this work.

Notes

The authors declare no competing financial interest.

■ ACKNOWLEDGMENTS

This work was supported by the NSFC (21725101, 21673213, and 21521001), the National Research Fund for Fundamental Key Project (2014CB931803), the Recruitment Program of Global Youth Experts, and the Fundamental Research Funds for the Central Universities (WK2060030029). We thank the staff of the BL17B beamline at the National Center for Protein Sciences Shanghai and Shanghai Synchrotron Radiation Facility (Shanghai, People's Republic of China) for assistance during single-crystal data collection.

■ REFERENCES

(1) Lewis, N. S.; Nocera, D. G. Powering the planet: chemical challenges in solar energy utilization. *Proc. Natl. Acad. Sci. U. S. A.* **2006**, *103*, 15729−15735.

(2) Chen, X.; Shen, S.; Guo, L.; Mao, S. S. Semiconductor-based photocatalytic hydrogen generation. *Chem. Rev.* **2010**, *110*, 6503−6570.

(3) Kudo, A.; Miseki, Y. Heterogeneous photocatalyst materials for water splitting. *Chem. Soc. Rev.* **2009**, *38*, 253−278.

(4) Zhang, T.; Lin, W. Metal−organic frameworks for artificial photosynthesis and photocatalysis. *Chem. Soc. Rev.* **2014**, *43*, 5982−5993.

(5) Zhang, J.; Chen, Y.; Wang, X. Two-dimensional covalent car-bon nitride nanosheets: synthesis, functionalization, and applications. *Energy Environ. Sci.* **2015**, *8*, 3092−3108.

(6) Zee, D. Z.; Chantarojsiri, T.; Long, J. R.; Chang, C. J. Metal−polypyridyl catalysts for electro- and photochemical reduction of water to hydrogen. *Acc. Chem. Res.* **2015**, *48*, 2027−2036.

(7) Furukawa, H.; Cordova, K. E.; O'Keeffe, M.; Yaghi, O. M. The chemistry and applications of metal-organic frameworks. *Science* **2013**, *341*, 1230444.

(8) Zhou, H.-C.; Kitagawa, S. Metal−organic frameworks (MOFs). *Chem. Soc. Rev.* **2014**, *43*, 5415−5418.

(9) Jiao, L.; Wang, Y.; Jiang, H.-L.; Xu, Q. Metal−organic frameworks as platforms for catalytic applications. *Adv. Mater.* **2017**, *30*, 1703663.

(10) Islamoglu, T.; Goswami, S.; Li, Z.; Howarth, A. J.; Farha, O. K.; Hupp, J. T. Postsynthetic tuning of metal−organic frameworks for targeted applications. *Acc. Chem. Res.* **2017**, *50*, 805−813.

(11) Li, B.; Wen, H.-M.; Cui, Y.; Zhou, W.; Qian, G.; Chen, B. Emerging multifunctional metal−organic framework materials. *Adv. Mater.* **2016**, *28*, 8819−8860.

(12) Zhou, T.; Du, Y.; Borgna, A.; Hong, J.; Wang, Y.; Han, J.; Zhang, W.; Xu, R. Post-synthesis modification of a metal-organic framework to construct a bifunctional photocatalyst for hydrogen production. *Energy Environ. Sci.* **2013**, *6*, 3229−3234.

(13) Pullen, S.; Fei, H.; Orthaber, A.; Cohen, S. M.; Ott, S. Enhanced photochemical hydrogen production by a molecular diiron catalyst incorporated into a metal−organic framework. *J. Am. Chem. Soc.* **2013**, *135*, 16997−17003.

(14) Sasan, K.; Lin, Q.; Mao, C.; Feng, P. Incorporation of iron hydrogenase active sites into a highly stable metal-organic framework for photocatalytic hydrogen generation. *Chem. Commun.* **2014**, *50*, 10390−10393.

(15) Wang, S.; Wang, X. Multifunctional metal-organic frameworks for photocatalysis. *Small* **2015**, *11*, 3097−3112.

(16) Dhakshinamoorthy, A.; Asiri, A. M.; García, H. Metal-organic framework (MOF) compounds: photocatalysts for redox reactions and solar fuel production. *Angew. Chem., Int. Ed.* **2016**, *55*, 5414−5445.

(17) An, Y.; Liu, Y.; An, P.; Dong, J.; Xu, B.; Dai, Y.; Qin, X.; Zhang, X.; Whangbo, M.-H.; Huang, B. NiII coordination to an Al-based metal-organic framework made from 2-aminoterephthalate for photocatalytic overall water splitting. *Angew. Chem., Int. Ed.* **2017**, *56*, 3036−3040.

(18) Dong, X.-Y.; Zhang, M.; Pei, R.-B.; Wang, Q.; Wei, D.-H.; Zang, S.-Q.; Fan, Y.-T.; Mak, T. C. W. A crystalline copper(II) coordination polymer for the efficient visible-light-driven generation of hydrogen. *Angew. Chem., Int. Ed.* **2016**, *55*, 2073−2077.

(19) Li, Z.; Xiao, J.-D.; Jiang, H.-L. Encapsulating a Co(II) molecular photocatalyst in metal-organic framework for visible-light-driven H_2 production: boosting catalytic efficiency via spatial charge separation. *ACS Catal.* **2016**, *6*, 5359−5365.

(20) Gomes Silva, C.; Luz, I.; Llabrés i Xamena, F. X.; Corma, A.; García, H. Water stable Zr−benzenedicarboxylate metal-organic frameworks as photocatalysts for hydrogen generation. *Chem. - Eur. J.* **2010**, *16*, 11133−11138.

(21) Wu, Z.-L.; Wang, C.-H.; Zhao, B.; Dong, J.; Lu, F.; Wang, W.-H.; Wang, W.-C.; Wu, G.-J.; Cui, J.-Z.; Cheng, P. A semi-conductive copper-organic framework with two types of photocatalytic activity. *Angew. Chem., Int. Ed.* **2016**, *55*, 4938−4942.

(22) Fu, Y.; Sun, D.; Chen, Y.; Huang, R.; Ding, Z.; Fu, X.; Li, Z. An amine-functionalized titanium metal-organic framework photo-catalyst with visible-light-induced activity for CO_2 reduction. *Angew. Chem., Int. Ed.* **2012**, *51*, 3364−3367.

(23) Laurier, K. G. M.; Vermoortele, F.; Ameloot, R.; De Vos, D. E.; Hofkens, J.; Roeffaers, M. B. J. Iron(III)-based metal-organic frameworks as visible light photocatalysts. *J. Am. Chem. Soc.* **2013**, *135*, 14488−14491.

(24) Zhang, H.; Wei, J.; Dong, J.; Liu, G.; Shi, L.; An, P.; Zhao, G.; Kong, J.; Wang, X.; Meng, X.; Zhang, J.; Ye, J. Efficient visible-light-driven carbon dioxide reduction by a single-atom implanted metal-organic framework. *Angew. Chem., Int. Ed.* **2016**, *55*, 14310−14314.

(25) Xu, H.-Q.; Hu, J.; Wang, D.; Li, Z.; Zhang, Q.; Luo, Y.; Yu, S.-H.; Jiang, H.-L. Visible-light photoreduction of CO_2 in a metal-organic framework: boosting electron-hole separation via electron trap states. *J. Am. Chem. Soc.* **2015**, *137*, 13440−13443.

(26) Shen, L.; Luo, M.; Huang, L.; Feng, P.; Wu, L. A clean and general strategy to decorate a titanium metal-organic framework with noble-metal nanoparticles for versatile photocatalytic applications. *Inorg. Chem.* **2015**, *54*, 1191−1193.

(27) Wang, C.; deKrafft, K. E.; Lin, W. Pt nanoparticles@photoactive metal-organic frameworks: efficient hydrogen evolution via synergistic photoexcitation and electron injection. *J. Am. Chem. Soc.* **2012**, *134*, 7211−7214.

(28) Fateeva, A.; Chater, P. A.; Ireland, C. P.; Tahir, A. A.; Khim-yak, Y. Z.; Wiper, P. V.; Darwent, J. R.; Rosseinsky, M. J. A water-stable porphyrin-based metal-organic framework active for visible-light photocatalysis. *Angew. Chem., Int. Ed.* **2012**, *51*, 7440−7444.

(29) Horiuchi, Y.; Toyao, T.; Saito, M.; Mochizuki, K.; Iwata, M.; Higashimura, H.; Anpo, M.; Matsuoka, M. Visible-light-promoted photocatalytic hydrogen production by using an amino-functionalized Ti(IV) metal-organic framework. *J. Phys. Chem. C* **2012**, *116*, 20848−20853.

(30) Wen, M.; Mori, K.; Kamegawa, T.; Yamashita, H. Amine-functionalized MIL-101(Cr) with imbedded platinum nanoparticles as a durable photocatalyst for hydrogen production from water. *Chem. Commun.* **2014**, *50*, 11645−11648.

(31) Xiao, J.-D.; Shang, Q.; Xiong, Y.; Zhang, Q.; Luo, Y.; Yu, S.-H.; Jiang, H.-L. Boosting photocatalytic hydrogen production of a metal-organic framework decorated with platinum nanoparticles: the platinum location matters. *Angew. Chem., Int. Ed.* **2016**, *55*, 9389−9393.

(32) Zheng, S.-T.; Zuo, F.; Wu, T.; Irfanoglu, B.; Chou, C.; Nieto, R. A.; Feng, P.-Y.; Bu, X. Cooperative assembly of three-ring-based

DOI: 10.1021/acscatal.8b00764
ACS Catal. 2018, 8, 4583−4590

zeolite-type metal-organic frameworks and Johnson-type dodecahedra. *Angew. Chem., Int. Ed.* **2011**, *50*, 1849−1852.
(33) Zhang, W.; Lai, W.; Cao, R. Energy-related small molecule activation reactions: oxygen reduction and hydrogen and oxygen evolution reactions catalyzed by porphyrin- and corrole-based systems. *Chem. Rev.* **2017**, *117*, 3717−3797.
(34) Han, Y.; Fang, H.; Jing, H.; Sun, H.; Lei, H.; Lai, W.; Cao, R. Singly versus doubly reduced nickel porphyrins for proton reduction: experimental and theoretical evidence for a homolytic hydrogen-evolution reaction. *Angew. Chem., Int. Ed.* **2016**, *55*, 5457−5462.
(35) Lei, H.; Fang, H.; Han, Y.; Lai, W.; Fu, X.; Cao, R. Reactivity and mechanism studies of hydrogen evolution catalyzed by copper corroles. *ACS Catal.* **2015**, *5*, 5145−5153.
(36) Mondal, B.; Sengupta, K.; Rana, A.; Mahammed, A.; Botoshansky, M.; Dey, S. M.; Gross, Z.; Dey, A. Cobalt corrole catalyst for efficient hydrogen evolution reaction from H_2O under ambient conditions: reactivity, spectroscopy, and density functional theory calculations. *Inorg. Chem.* **2013**, *52*, 3381−3387.
(37) Mahammed, A.; Mondal, B.; Rana, A.; Dey, A.; Gross, Z. The cobalt corrole catalyzed hydrogen evolution reaction: surprising electronic effects and characterization of key reaction intermediates. *Chem. Commun.* **2014**, *50*, 2725−2727.
(38) Johnson, J. A.; Zhang, X.; Reeson, T. C.; Chen, Y.-S.; Zhang, J. Facile control of the charge density and photocatalytic activity of an anionic indium porphyrin framework via in situ metalation. *J. Am. Chem. Soc.* **2014**, *136*, 15881−15884.
(39) Johnson, J. A.; Luo, J.; Zhang, X.; Chen, Y.-S.; Morton, M. D.; Echeverría, E.; Torres, F. E.; Zhang, J. Porphyrin-metalation-mediated tuning of photoredox catalytic properties in metal-organic frameworks. *ACS Catal.* **2015**, *5*, 5283−5291.
(40) Xu, L.; Zhai, M.-K.; Lu, X.-C.; Du, H.-B. A robust indium−porphyrin framework for CO_2 capture and chemical transformation. *Dalton Trans.* **2016**, *45*, 18730−18736.
(41) Fateeva, A.; Clarisse, J.; Pilet, G.; Grenèche, J.-M.; Nouar, F.; Abeykoon, B. K.; Guegan, F.; Goutaudier, C.; Luneau, D.; Warren, J. E.; Rosseinsky, M. J.; Devic, T. Iron and porphyrin metal-organic frameworks: insight into structural diversity, stability, and porosity. *Cryst. Growth Des.* **2015**, *15*, 1819−1826.
(42) Feng, D.; Gu, Z.-Y.; Li, J.-R.; Jiang, H.-L.; Wei, Z.; Zhou, H.-C. Zirconium-metalloporphyrin PCN-222: mesoporous metal-organic frameworks with ultrahigh stability as biomimetic catalysts. *Angew. Chem., Int. Ed.* **2012**, *51*, 10307−10310.
(43) Sheldrick, G. M. *SHELXS-97, Programs for X-ray Crystal Structure Solution*; University of Göttingen: Göttingen, Germany, 1997.
(44) Sheldrick, G. M. *SHELXL-97, Programs for X-ray Crystal Structure Refinement*; University of Göttingen: Göttingen, Germany, 1997.
(45) Dolomanov, O. V.; Bourhis, L. J.; Gildea, R. J.; Howard, J. A. K.; Puschmann, H. OLEX2: a complete structure solution, refinement and analysis program. *J. Appl. Crystallogr.* **2009**, *42*, 339−341.
(46) Spek, A. L. Single-crystal structure validation with the program PLATON. *J. Appl. Crystallogr.* **2003**, *36*, 7−13.
(47) Valicsek, Z.; Horváth, O.; Lendvay, G.; Kikaš, L.; Škorić, L. Formation, photophysics, and photochemistry of cadmium(II) complexes with 5,10,15,20-tetrakis(4-sulfonatophenyl)porphyrin and its octabromo derivative: The effects of bromination and the axial hydroxo ligand. *J. Photochem. Photobiol., A* **2011**, *218*, 143−145.
(48) Fleischer, E. B.; Wang, J. H. The detection of a type of reaction intermediate in the combination of metal ions with porphyrins. *J. Am. Chem. Soc.* **1960**, *82*, 3498−3502.
(49) Barkigia, K. M.; Fajer, J.; Adler, A. D.; Williams, G. J. B. Crystal and molecular structure of (5,10,15,20-tetra-N-propylporphinato)lead-(II): a "roof" porphyrin. *Inorg. Chem.* **1980**, *19*, 2057−2061.
(50) Lin, Z.; Zhang, Z.-M.; Chen, Y.-S.; Lin, W. Highly efficient cooperative catalysis by CoIII (porphyrin) pairs in interpenetrating metal-organic frameworks. *Angew. Chem., Int. Ed.* **2016**, *55*, 13739−13743.
(51) Horváth, O.; Valicsek, Z.; Harrach, G.; Lendvay, G.; Fodor, M. A. Spectroscopic and photochemical properties of water-soluble metalloporphyrins of distorted structure. *Coord. Chem. Rev.* **2012**, *256*, 1531−1545.
(52) Aguirre-Díaz, L. M.; Reinares-Fisac, D.; Iglesias, M.; Gutiérrez-Puebla, E.; Gándara, F.; Snejko, N.; Monge, M. Á. Group 13th metal-organic frameworks and their role in heterogeneous catalysis. *Coord. Chem. Rev.* **2017**, *335*, 1−27.
(53) Duan, J.; Jin, W.; Kitagawa, S. Water-resistant porous coordination polymers for gas separation. *Coord. Chem. Rev.* **2017**, *332*, 48−74.
(54) Guo, Z.-J.; Yu, J.; Zhang, Y.-Z.; Zhang, J.; Chen, Y.; Wu, Y.; Xie, L.-H.; Li, J.-R. Water-stable In(III)-based metal-organic frameworks with rod-shaped secondary building units: single-crystal to single-crystal transformation and selective sorption of C_2H_2 over CO_2 and CH_4. *Inorg. Chem.* **2017**, *56*, 2188−2197.
(55) Valicsek, Z.; Horváth, O. Formation, photophysics and photochemistry of thallium(III) 5,10,15,20-tetrakis(4-sulphonatophenyl)porphyrin: New supports of typical sitting-atop features. *J. Photochem. Photobiol., A* **2007**, *186*, 1−7.
(56) Wang, C.; deKrafft, K. E.; Lin, W. Pt nanoparticles@photoactive metal-organic frameworks: efficient hydrogen evolution via synergistic photoexcitation and electron injection. *J. Am. Chem. Soc.* **2012**, *134*, 7211−7214.
(57) Kim, D.; Whang, D. R.; Park, S. Y. Self-healing of molecular catalyst and photosensitizer on metal−organic framework: robust molecular system for photocatalytic H_2 evolution from water. *J. Am. Chem. Soc.* **2016**, *138*, 8698−8701.
(58) Hou, C.-C.; Li, T.-T.; Cao, S.; Chen, Y.; Fu, W.-F. Incorporation of a $[Ru(dcbpy)(bpy)_2]^{2+}$ photosensitizer and a $Pt(dcbpy)Cl_2$ catalyst into metal−organic frameworks for photocatalytic hydrogen evolution from aqueous solution. *J. Mater. Chem. A* **2015**, *3*, 10386−10394.
(59) Zheng, N.; Zhang, J.; Bu, X.; Feng, P. Cadmium-porphyrin coordination networks: rich coordination modes and three-dimensional four-connected $CdSO_4$ and (3,5)-connected hms nets. *Cryst. Growth Des.* **2007**, *7*, 2576−2581.

DOI: 10.1021/acscatal.8b00764
ACS Catal. 2018, 8, 4583−4590